

On the Formation of Defects and Morphology during Chemical Vapor Deposition of Tungsten

Ji-Tao Wang,* Chuan-Bao Cao, and Hao Wang

Department of Electronic Engineering, Fudan University, 200433 Shanghai, China

Shi-Li Zhang

Royal Institute of Technology-Electrum, Solid State Electronics, S-164 28 Kista, Sweden

ABSTRACT

Face-to-face wafers were used to observe anomalous tungsten deposition in the gap-edge between wafers. In the WF_6 - H_2 atmosphere, three regions are identified: (i) an open-deposition region (region A), (ii) a half-sealed deposition region (region B), and (iii) an etching or tunnel region (region C). In the WF_6 -Ar atmosphere, there are only two regions: (i) an open deposition region (region A'), and (ii) a half-sealed deposition region (region B'). The third region disappears because HF does not form in the absence of H_2 . Different chemical reactions are expected in different regions, dictated by the local gas composition. A half-sealed structure model proposed here is supported by thermodynamic calculations, and applied to explain encroachment, wormholes, and other well-known effects during the chemical vapor deposition of tungsten from tungsten hexafluoride.

The chemical vapor deposition of tungsten (CVD-W) process is attractive for ultralarge scale integration (ULSI) technology.^{1,2} For multilevel interconnection applications, both blanket and selective deposition of tungsten (W) films can be used. It is common knowledge that the CVD-W process is sensitive to the surface condition and thus to the precleaning processes prior to the deposition. Various abnormal phenomena and microstructures in submicrometer dimensions have been observed. These include the self-limiting nature of the W growth by silicon (Si) reduction of tungsten hexafluoride (WF_6), the surface and interface roughness, the formation of microtunnels (wormholes), the formation of encroachment, the oxygen and fluorine accumulation at the W/Si interface, and the oxygen residuals between the hydrogen (H_2)-reduced and Si-reduced W layers, etc.³⁻¹² Different mechanisms have been proposed to explain these phenomena. However, a consistent interpretation of the observations is not yet available in the literature, despite many publications. Thus, this paper is devoted to systematically establishing a half-sealed structure model which can explain consistently all the above-mentioned observations documented in the literature.¹³⁻¹⁶ We show that these phenomena are intimately related and can be traced back to a common formation mechanism.

Experimental

Both cold-wall and hot-wall low pressure CVD reactors were used for sample preparation for comparison. Argon (Ar, 99.9999%), H_2 (99.9999%), and WF_6 (99.8%) were employed as the reactants or carrier gas. Silicon wafers of both n-type (phosphorus-doped) and p-type (boron-doped), and of <100>-orientation, were always loaded at room temperature (<30°C). During ramping up the substrate temperature, the Si surface was protected by purging it in H_2 or Ar. When a stabilized temperature was established, 6 sccm WF_6 and 200 sccm H_2 or Ar were introduced. The base pressure of the reactors was lower than 0.1 Pa and the total pressure during deposition was 100 Pa. When the deposition procedure was ended, the whole system was then cooled down to room temperature under the H_2 or Ar gas protection, before unloading the wafer. The deposition time was 15 min, unless specified otherwise.

The samples were prepared as follows. A smaller bare Si wafer or an oxidized Si wafer partly covered a bare Si wafer face-to-face. Both the bare Si wafers were etched in a 1% hydrogen fluoride (HF) solution, rinsed in deionized water, and blow-dried by nitrogen gas immediately prior to W deposition. The oxidized Si wafer had a 750 nm (wet) thermal oxide on its surface, therefore it was cleaned only

* Electrochemical Society Active Member.

in deionized water before being loaded into the reactor. Designed in this way, the surface region on the lower big wafer close to the periphery of the upper covering wafer constituted the most important part of the study.

Besides this configuration, ordinary (no covering wafer) Si wafers with and without native oxide were used for W deposition. Samples were analyzed by alpha-step meter, scanning electron microscope (SEM), and x-ray fluorescence (XRF).

Results

On ordinary Si wafers.—The W thickness on ordinary (no covering wafer) Si wafers with and without native oxide was measured by XRF. In the presence of H_2 , the thickness of W films deposited on the Si wafer without native oxide was 11.7 nm, while that on the Si wafer with native oxide was 29.0 nm. In the absence of H_2 but with Ar as the carrier gas, the W films on Si wafers without native oxide were 10.8 nm thick after 15 min deposition and 9.2 nm after 180 min deposition, a typical result of self-limiting deposition of W.

On partly protected Si wafers.—The upper covering wafer was taken away after the deposition. An alpha-step meter was used for mapping the surface morphology of the Si wafer of larger dimension. Figures 1a-d illustrate typical results obtained from samples prepared in the WF_6 - H_2 atmosphere. Three regions are identified for all these figures. Region A represents an open-deposition area, where the Si surface was exposed to the main gas flow during deposition and only thin W films were deposited. The W deposition rate of H_2 reduction in region A for these particular samples was lower than 1.0 nm/min. Region B is the half-sealed deposition region, which was the surface area close to the periphery of the upper covering wafer of smaller dimension, but still under it. A much thicker W layer ca. 200 nm was deposited in this region, and a deposition rate of H_2 reduction in region B greater than 12 nm/min was found. Finally, region C represents an etch area under the upper covering wafer of smaller dimension. Here, a dip, observed by the eyes as a black line in the Si surface, was detected, indicating Si etching in this area. The maximum depth of the dip was ca. 120 nm (Fig. 1a-d). The area far toward the right-hand side of these figures was the center under the smaller covering wafer, and the original Si surface there did not change during the deposition.

The comparison between the depositions on n- and p-type Si substrates (Fig. 1a vs. Fig. 1c and Fig. 1b vs. Fig. 1d, respectively) shows no obvious difference. There is, however, a difference between the degree of the Si substrate etching under the bare Si wafer and that under the thick

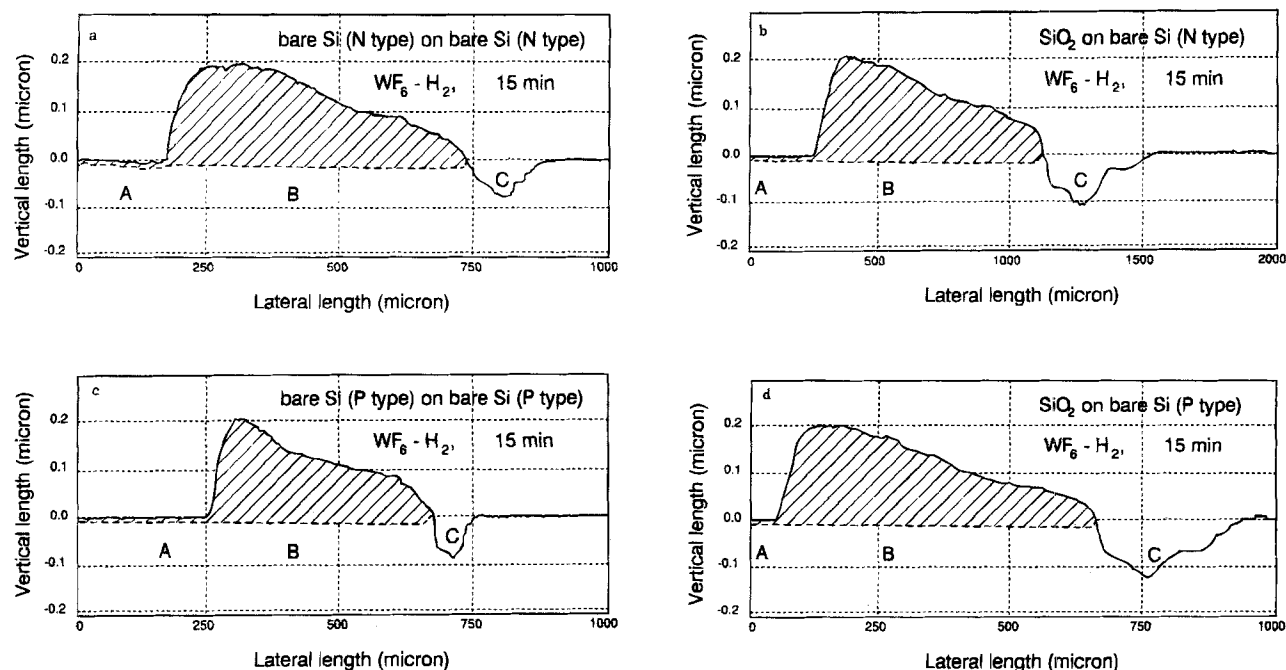


Fig. 1. (a to d) Surface morphology of the samples prepared in WF_6-H_2 for 15 min.

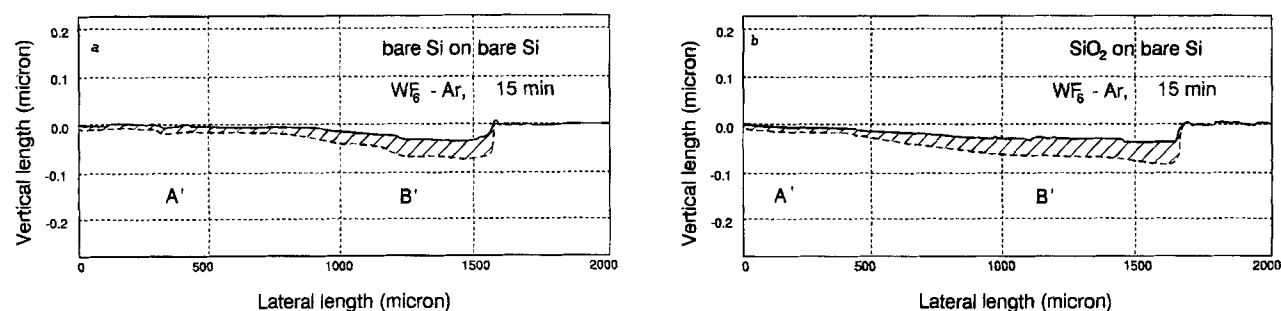


Fig. 2. (a and b) Surface morphology of the samples prepared in WF_6-Ar for 15 min.

oxide wafer in region C (Fig. 1a vs. Fig. 1b for n-type and Fig. 1c vs. Fig. 1d for p-type, respectively); more erosion in the Si substrate is found in the ordinary Si wafer under the thick oxide covering wafer.

Figures 2a and 2b depict the deposition results prepared in the WF_6-Ar atmosphere. The etching or tunneling region completely disappears and only the open-deposition region (region A') and the half-sealed deposition region (region B') are present. The depth in region B' (*i.e.*, the height from the W surface) was about 40 nm, which is a consequence of the volume shrinkage of Si reduction.

Prolonging the deposition time from 15 to 180 min in the same WF_6-Ar atmosphere, the depth in the half-sealed deposition region (region B') increased to 130 nm, while the W thickness in region A' was essentially the same as that after the 15 min deposition, as shown in Fig. 3a and b. This indicates the deposition in the half-sealed deposition region (region B') of the WF_6-Ar atmosphere is not self-limiting.

Surface morphology.—The W films formed in region A are very smooth, observed by SEM (Fig. 4a). This was the same for the W deposited on bare Si wafers without native oxide. The W films deposited in region B (Fig. 4b) or deposited on ordinary Si wafers with native oxide are very rough.

Thermodynamic Calculations

To understand the above experimental observations, some relevant equilibrium systems are considered below. The thermodynamic data of the substances used in the calculations are the same as in Ref. 17. Figure 5 is the phase

diagram for the interaction between WF_6 and silicon dioxide (SiO_2) and Fig. 6 shows the corresponding equilibrium gas composition.

The input substances used for the equilibrium calculations consisted of one gas species (WF_6) and one solid phase (SiO_2). In reality the interaction between WF_6 and SiO_2 only occurs on the SiO_2 surface, since substantial diffusion of WF_6 into the SiO_2 bulk is not likely to take place. Hence, the amount of SiO_2 which takes part in the reaction is expected to be small. The calculations also must cover the range of small molar ratios of the solid substance to the gas species. Based on the calculations, if the initial molar ratio of SiO_2/WF_6 is in the range below 0.5 to 1, dependent on temperature, only the gas products are produced (Fig. 5). As seen in Fig. 6, tungsten oxytetrafluoride (WOF_4) predominates the gaseous reaction products over the whole range of the initial SiO_2 to WF_6 molar ratios used for the calculations, although silicon tetrafluoride (SiF_4) is also an important gas species. Therefore, the overall chemical reaction under such conditions may be simplified as



Further calculations were carried out to study the interaction between WOF_4 and W (Fig. 7) and between WOF_4 and Si (Fig. 8). In both chemical systems, *i.e.*, the WOF_4-W and WOF_4-Si interactions, the solid tungsten oxytrifluoride (WOF_3) almost always is formed. The formation of WOF_3 is important in the CVD-W process, and is discussed later.

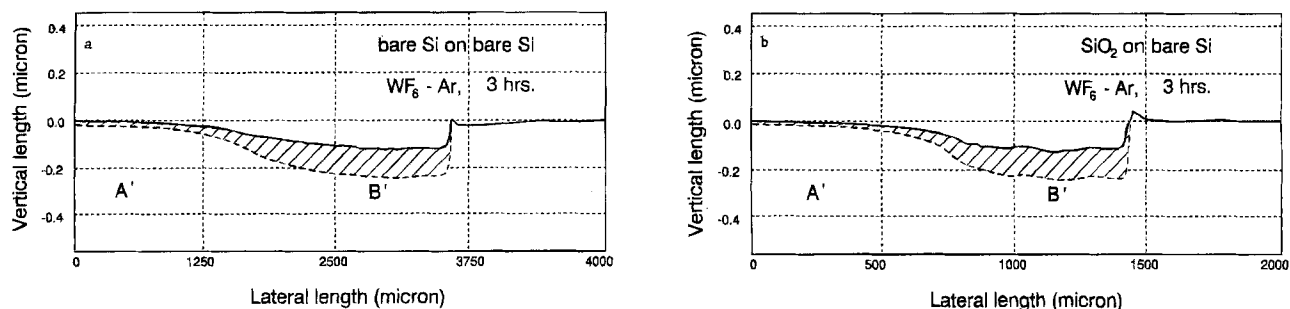


Fig. 3. (a and b) Surface morphology of the samples prepared in WF_6 -Ar for 180 min.

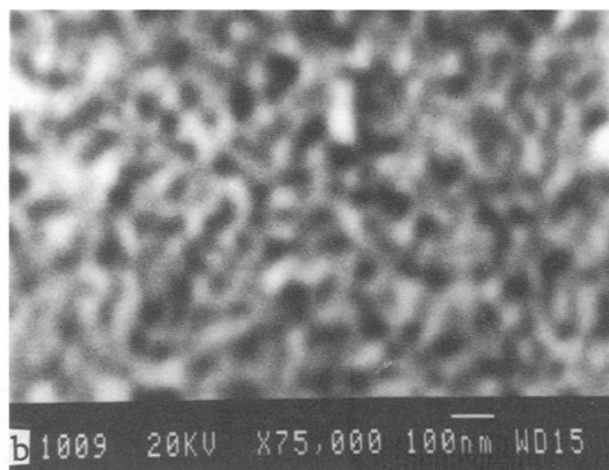
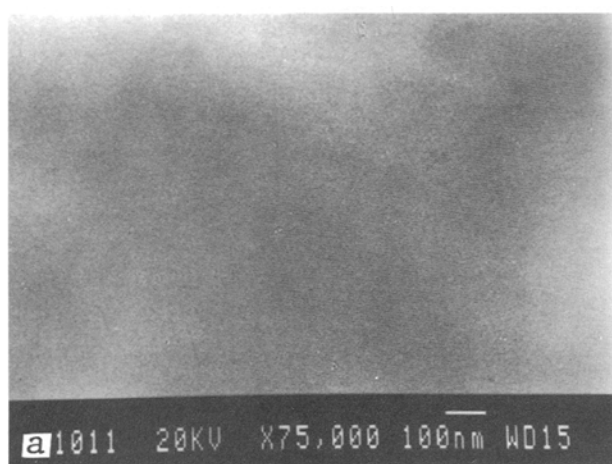
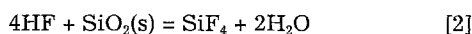


Fig. 4. (a and b) SEM pictures showing the morphology of the W film surfaces.

The equilibrium gas composition of the interaction between HF and SiO_2 (*i.e.*, etching of SiO_2 by HF) was calculated under the same conditions of 100 Pa and 300°C. The results are shown in Fig. 9 and the overall chemical reaction can be written as



The Half-Sealed Structure Model

The experimental results shown in Fig. 1 through 3 clearly suggest that different chemical reactions prevail in different regions, both for the WF_6 - H_2 and the WF_6 -Ar atmosphere. In the open-deposition region of the WF_6 -Ar atmosphere (region A'), the Si reduction of WF_6 is self-limiting. This is not so in the half-sealed deposition region of the WF_6 -Ar atmosphere (region B'), and longer deposition time results in thicker W layers (Fig. 3 *vs.* Fig. 2). For the WF_6 - H_2

atmosphere, the interaction between WF_6 and Si predominates the initial deposition until a certain thick W layer is formed, and thereafter the H_2 reduction of WF_6 takes over. The W deposition rate of H_2 reduction in the half-sealed deposition region of the WF_6 - H_2 atmosphere (region B) is much higher than that in the open-deposition region (region A). Moreover, the appearance of the Si etching region (region C) is closely related to the involvement of hydrogen (Fig. 1).

Based on these results as well as the thermodynamic calculations, a half-sealed structure model now is systematically proposed. Because of volume shrinkage in the W deposition by Si reduction of WF_6 (a factor of about 1.9), half-sealed structures are easy to form under native oxide or at the corner of patterned oxide windows.^{3,5} Inside the structures, the mass transport of the gas molecules is limited. Then,

1. The gas composition inside the structure is assumed to be different from that in the bulk vapor atmosphere. The concentration of tungsten subfluorides, WF_n ($n = 1, \dots, 5$), then is higher inside the structures. In the presence of H_2 , HF also must be considered.

2. Referring to the thermodynamic calculations, the formation of a solid tungsten oxyfluoride, WOF_3 , is favored in the presence of a trace of oxygen. This compound is thermodynamically stable under the experimental conditions used here. Thus, we assume that the formation of WOF_3 is the major cause responsible for the self-limiting nature of the W deposition by Si reduction. WOF_3 is a diffusion barrier for WF_6 . Considering the smaller molecular size and the more active nature of WF_n ($n = 1, \dots, 5$), they, to some extent, can penetrate through WOF_3 .

Therefore, the predominant reactions in different regions in the WF_6 - H_2 atmosphere may be expressed as below.

In the open deposition region (region A).—

(i) For the W deposition

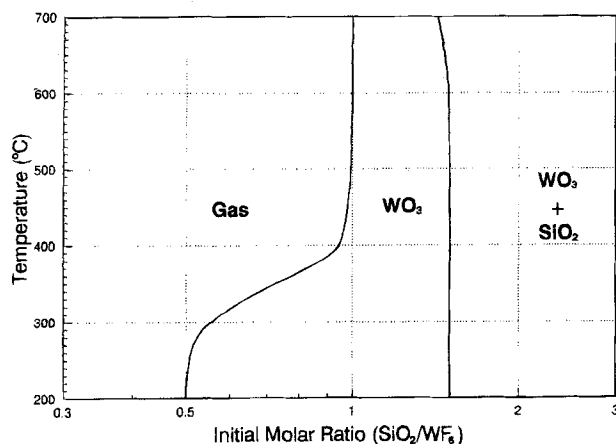
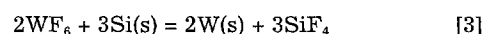
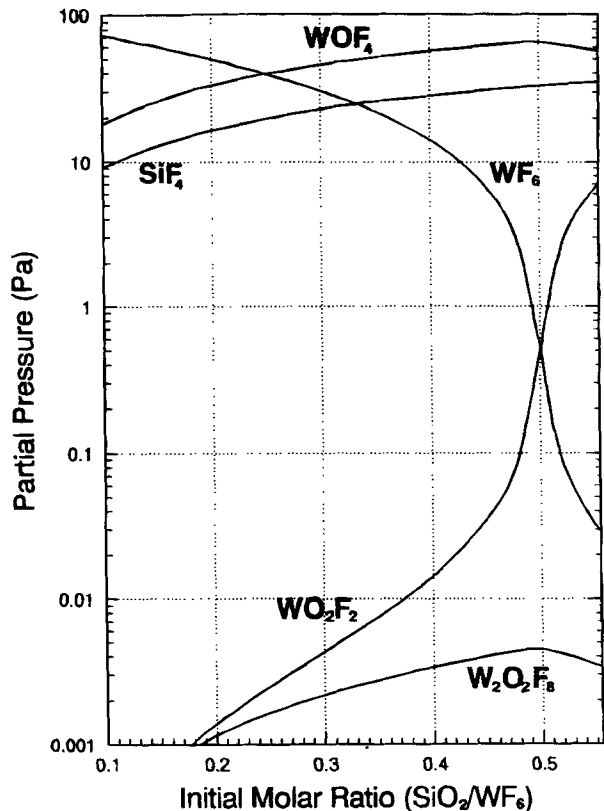
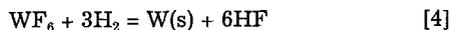


Fig. 5. Phase diagram of the SiO_2 - WF_6 system. Total pressure: 100 Pa.

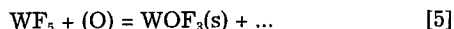


Total Pressure = 100 Pa, T = 300°C

Fig. 6. Equilibrium gas composition of the SiO₂-WF₆ system.



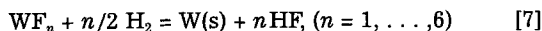
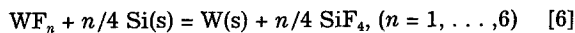
(ii) For the formation of oxyfluorides, which is relative to the self-limited W growth



Oxygen in trace quantity can be a result of leakage, oxygen-containing impurities in gases, or gas residuals in the reaction chamber.

In the half-sealed deposition region (region B).—

(i) For the W deposition



The tungsten subfluorides (i.e., WF_n, n = 1, ..., 5) are anticipated to be more chemically reactive than WF₆. Thus,

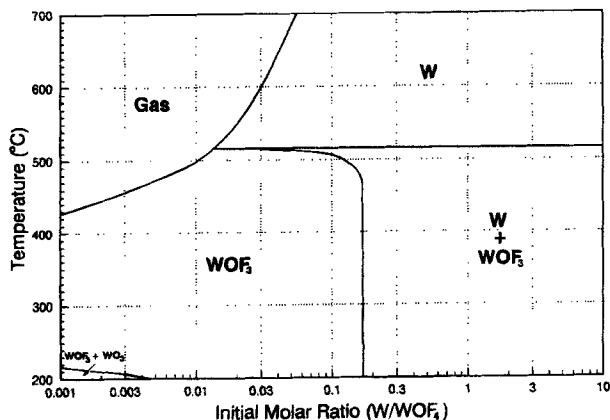


Fig. 7. Phase diagram of the W-WOF₄ system. Total pressure: 100 Pa.

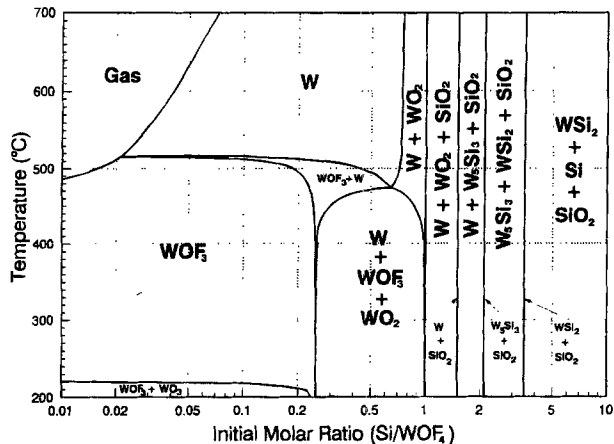
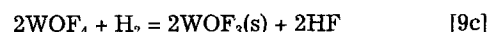
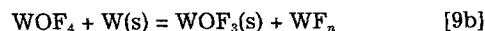
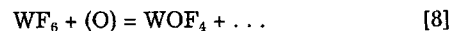


Fig. 8. Phase diagram of the Si-WOF₄ system. Total pressure: 100 Pa.

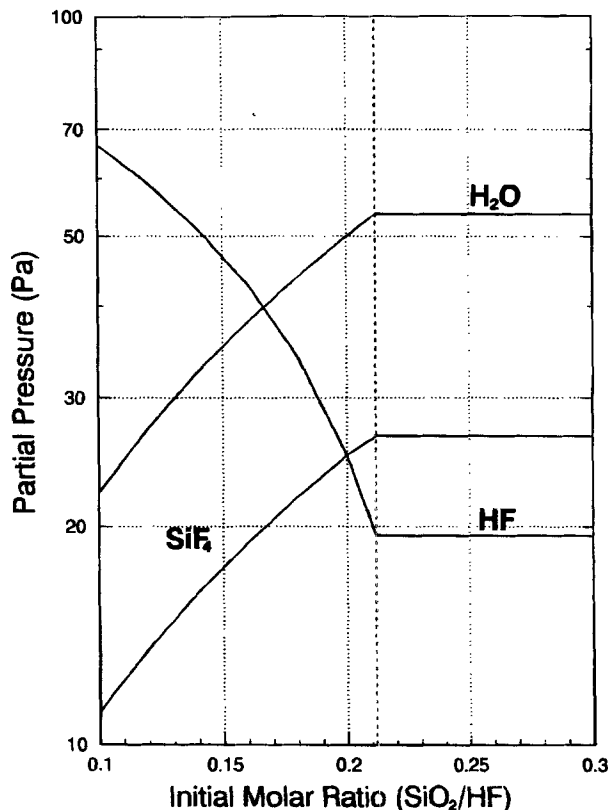
higher deposition rates are expected in region B than in region A, which has been seen in Fig. 1a-d.

(ii) For the formation of oxyfluorides (in addition to reactions 1 and 5



(iii) The interaction between SiO₂ and fluorides

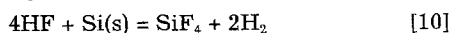
Besides SiO₂ etching by WF₆ and HF (i.e., reactions 1 and 2), some reactions between tungsten subfluorides, WF_n (n = 1, ..., 5), and oxide can take place.



Total Pressure = 100 Pa, T = 300°C

Fig. 9. Equilibrium gas composition of the SiO₂-HF system.

In the etching region (region C).—



The predominant reactions in different regions of the WF_6 -Ar atmosphere (region A' and region B') basically are the same chemical reactions as in corresponding region A and region B of the WF_6 - H_2 atmosphere, but those reactions involving hydrogen, *i.e.*, reactions 4, 7, 9c, and 10, are excluded.

Now, the half-sealed structure model can be used to discuss our experimental results. In our experiment, when one Si wafer is lying on the other, the interval between the wafers is very small, sufficient for forming a half-sealed structure. The mass transport of the gas molecules is limited in this area between the two wafers. Thus, a different gas composition is anticipated in this region from that in the bulk vapor atmosphere. However, this interval is considered far beyond (*i.e.*, much larger than) the submicrometer range where the various features have been observed frequently. This explains the much larger dimensions (on the order of hundreds, and even a thousand, micrometers) for the W formation in region B or region B' and the Si etching in region C, as compared with the corresponding observations in the literature.³⁻¹⁰

In the presence of H_2 , the low deposition rate of H_2 reduction in region A essentially may be accomplished by H_2 reduction of WF_6 . In region B, the high deposition rate of H_2 reduction may be a result of H_2 reduction of WF_n ($n = 1, \dots, 5$). In region C, the highly concentrated HF may etch Si rapidly, and tunnels (wormholes) are formed.

In the absence of H_2 , the deposition of W in region A' is self-limiting, because of the diffusion barrier WOF_3 to WF_6 . In region B', the highly concentrated WF_n ($n = 1, \dots, 5$) may penetrate the barrier, leading to more W deposition. Since no hydrogen is present, the etching region is not found, as expected. Thus, no tunnels or wormholes are observed in the WF_6 -Ar atmosphere.

Further Applications of the Model

Self-limiting nature of W deposition by Si reduction.—W deposition by Si reduction of WF_6 has been shown to be a self-limiting process.³⁻¹⁰ Lifshitz proposed that there existed a passivation compound which was responsible for the self-limiting effect in the W deposition.¹⁰ The compound which forms a continuous layer or is mixed with pure deposited W was further suggested to be tungsten tetrafluoride (WF_4). WF_4 was assumed to be a nonvolatile compound under the experimental conditions commonly used. Based on our thermodynamic studies, this passivation compound is WOF_3 .

Thermodynamic calculations predict that WOF_3 is vaporized above 300°C under ultrahigh vacuum (UHV) conditions. Therefore, the W deposition by Si reduction of WF_6 under UHV conditions may result in unlimited depositions.¹⁸ In Ref. 18, the unlimited deposition of W in a cold-wall low pressure CVD reactor was reported. However, oxygen (20 to 25%) was present in the so-called as-deposited Si-reduced W film (see Fig. 4a in Ref. 18). It was a WO_x film, not a W film. The large amount of oxygen due to the leakage upstream may oxidize WOF_3 .

SiO_2 - WF_6 interaction in the presence of H_2 .—The reactivity of SiO_2 in the WF_6 - H_2 atmosphere has been controversial. A recent publication claimed that there was no evidence of any interfacial reaction between SiO_2 and WF_6 during W deposition by H_2 reduction of WF_6 .¹⁹ The formation of voids at the W/ SiO_2 interface was revealed in the same article by transmission electron microscopy (TEM) (see Fig. 12 in Ref. 19). No explanation for the void formation was given.

In our model, the half-sealed structures may be surrounded by solid phases other than Si and SiO_2 . Thus, together with the underlying SiO_2 , the hill-like W deposits on SiO_2 provide the necessary environment for forming the half-sealed structures there. Referring to the model, the concentration of WF_n ($n = 1, \dots, 5$) and HF may be sufficiently high inside the structures (partly sealed by the W crystals) to etch SiO_2 and form voids.

Formation of wormholes in the presence of H_2 .—Stocy *et al.* suggested that the W particles at the end of wormholes played a role in catalyzing the reaction between Si and fluoride compounds produced from the reaction of WF_6 and Si.⁴ SiF_4 now is the primary reaction product. Paine *et al.* proposed another mechanism attributing the wormhole formation as a result of the interaction between Si and HF.¹² Green *et al.* further ascribed the formation of wormholes as the catalytic gasification of Si by HF.⁸ However, some questions remain unanswered.

Generally, the wormholes or tunnels are found under thick native oxide or in the corner regions where SiO_2 , Si, and W meet.^{4,5,8,12} Moreover, the W particles at the end of the tunnels are neither consumed nor enlarged during the tunnel formation.

According to our model and the experimental observations in Fig. 1, wormholes may form only in the etching region (region C), *i.e.*, close to the end of the half-sealed structures. In this region, gaseous W compounds essentially are depleted. Occasionally, new nuclei of W particles may form on the Si surface from trace tungsten fluorides, and then tunnels may start to grow. Since HF does not etch the W deposits formed under our experiment conditions substantially, the W particles at the end of the tunnels must be kept constant in size.

Formation of encroachment.—Because of the volume shrinkage during W deposition from Si reduction of WF_6 , the interaction between Si and WF_6 at the foot of a patterned oxide window leads to the formation of encroachment under the oxide, which is a perfect half-sealed structure. Pictures of such encroachments are available in the literature (see, for instance, Fig. 2b in Ref. 5). Similar encroachment morphology can be seen in Fig. 2 and 3 of this paper, if the upper small Si wafer should be included in the drawings. Encroachment also may form in the presence of H_2 , and the void is later filled by W deposits, or left unfilled as the inlet of the encroachment structure is completely sealed by W deposited by the H_2 reduction of WF_6 .⁷

Oxide residuals between the Si reduced and H_2 reduced W layers.—In the presence of H_2 , W deposition begins with the Si reduction of WF_6 and W grows under a thin native oxide (<2 nm) through pinholes. A half-sealed structure is then formed. When the thin oxide layer is etched through inside out by the interactions between SiO_2 and WF_n ($n = 1, \dots, 6$) as well as between the SiO_2 and HF, the half-sealed structure is destroyed and the Si reduction is terminated. The W deposition continues with H_2 reduction of WF_6 and the rest of the oxide layer is buried. Hence, some oxide residuals may be left between the Si-reduced and H_2 -reduced W layers. Figure 2 in Ref. 4 gives excellent evidence of such oxide residuals.

In the absence of H_2 , such phenomena are not expected, referring to our model.

Fluorine and oxygen accumulation at the W/Si interface.—It has been reported that after W deposition, fluorine and oxygen were accumulated at the W/Si interface.^{6,10,11} According to our thermodynamic studies, solid state W-O-F compounds such as WOF_3 are stable under the experimental conditions commonly used in W deposition. Native oxide on the Si surface and the trace of oxygen in ordinary CVD processes is inevitable and provides the oxygen source for the formation of the W-O-F compounds in the beginning of the W deposition.

Influence of native oxide on W deposition.—Busta and Tang conducted a systematic study on the influence of native oxide on W deposition.⁶ When the native oxide is *ca.* 0.5 and 2 nm thick, the self-limiting thicknesses of the deposited W films are 10 and 200 nm, respectively. Broadbent *et al.* proposed a pinhole model earlier to explain the dependence of the W film thickness on native oxide.³ However, it was later pointed out by Green *et al.* that the pinhole model does not provide a satisfactory picture to reveal the relationship between the thickness of native oxide and that of the deposited W.⁸ Referring to the pinhole model, the

vertical W growth under each pinhole is self-limited and only proceeds laterally under native oxide. Only a few monolayers of the continuous W film are sufficient to terminate further W growth by Si reduction, as the W growth on a clean Si surface. This is contrary to the experimental observations. Moreover, the W films were not continuous, according to TEM observation.⁸

This phenomenon can be interpreted using the half-sealed structure model. On a clean Si surface, the Si reduction of WF_6 quickly ceases to proceed over the whole Si surface, because of the formation of a mixed W film (of ca. 10 nm thickness) which in turn is covered by a passivation WOF_3 layer or consists of W and WOF_3 . WF_6 molecules are not able to penetrate through WOF_3 . Such depositions always end up with a smooth W surface and a sharp W/Si interface. This corresponds to the W deposition in the open-deposition region (region A or region A' in Fig. 1 to 3).

When a thin native oxide film is present on the Si surface, the deposition reaction begins in the pinholes of native oxide. Microhalf-sealed structures are then formed under thin native oxide, again because of the volume shrinkage associated with the Si reduction. The half-sealed structures limit the mass transport of the reaction intermediates, i.e., WF_n ($n = 1, \dots, 5$), and thus keep a much higher concentration of the intermediates inside the structures than in the bulk vapor atmosphere. A thicker W film forms, because WF_n ($n = 1, \dots, 5$) can penetrate through WOF_3 . Since the penetration can be nonuniform, the W/Si interface as well as the W surface can be very rough. This has been seen in the half-sealed deposition region (region B or region B') in our experiment (Fig. 1 to 3). At the same time during W growth, native oxide is etched away gradually by the tungsten fluorides, i.e., WF_n ($n = 1, \dots, 6$) (and HF, if in the presence of H_2). As the native oxide film is consumed, the half-sealed structure is destroyed and the concentrations of WF_n ($n = 1, \dots, 6$) resume the same values as in the bulk vapor atmosphere. The Si reduction is then interrupted. Therefore, in general the thicker the native oxide (but still < 2 nm), the longer the Si reduction process lasts, then the thicker the self-limiting thickness of W layer and the rougher the W surface and W/Si interface are.

If the native oxide is too thick (> 2 nm), WF_6 is depleted before it reaches the Si substrate through the pinholes. No W films may be deposited now, which shows the deposition selectivity of the process.

The history effect of the pretreatment, the thickness ratio of the consumed Si to the forming W in Si reduction of WF_6 , the kinetics and conformal deposition for filling deep via windows all can be connected with the half-sealed structure model.

There is a fundamental difference between the half-sealed structure model and the pinhole model. The former takes into consideration the important role of subfluorides and the chemical reaction between SiO_2 and fluorides as the W growth proceeds under each pinhole. Thus, the half-sealed structures may be destroyed when the SiO_2 is being etched through inside out. This process is presented schematically in Fig. 10.

Conclusion

A half-sealed structure model has been proposed to explain the self-limiting nature in selective W deposition and the formation of some defects and morphological characters. Because of the presence of the surrounding materials (i.e., Si, SiO_2 , W, etc.), the exchange between the vapor phase inside the half-sealed structures and that in the bulk vapor atmosphere is limited, thus different gas compositions are expected. Consequently, different chemical reactions may be expected in different regions. In the presence of H_2 , there are three regions: (i) the open-deposition region (region A), (ii) the half-sealed deposition region (region B), and (iii) the etching or tunneling region (region C). The deposition rate by H_2 reduction was much higher in region B than that in the usual open-deposition region. Wormholes only form in the etching region at the end of the W deposits. However, in the absence of H_2 , two reaction regions were identified. (i) In the open-deposition region (re-

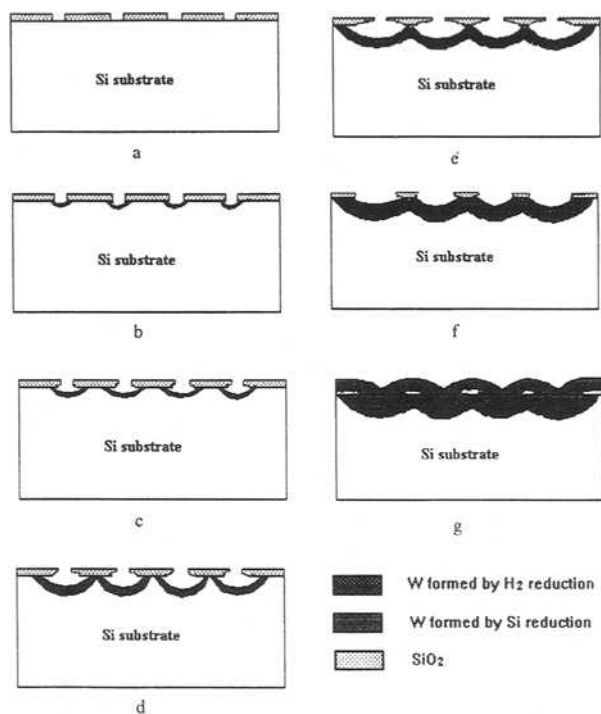


Fig. 10. Schematic diagram of the half-sealed structure model for the W deposition on an Si substrate with a thin native oxide.

gion A'), the Si reduction is self-limiting and (ii) in the half-sealed deposition region (region B'), a time-dependent W deposition of Si reduction was obtained. The tungsten subfluorides play an important role in the half-sealed structure (region B or region B'). The half-sealed structure model was used to interpret the morphology of encroachment in the WF_6 -Ar atmosphere and other observations in the W deposition, e.g., the accumulation of fluorine and oxygen at the W/Si interface, the oxide residuals between the Si reduced and H_2 reduced W layers, etc.

Acknowledgment

This work was supported partly by the National Natural Science Foundation of China (Grant No. 69276020) and the Swedish Broad for Technical Development. Professor J.-O. Carlsson of Uppsala University, Sweden, is gratefully acknowledged. Thanks are due also to B. Noland and T. Andersson of Uppsala University, Professor G.-Y. Wu and Y.-L. Hao of Beijing University for their help.

Manuscript submitted Nov. 12, 1993; revised manuscript received March 22, 1994. This was Papers 1249 and 1272 presented at the Honolulu, HI, Meeting of the Society, May 16-21, 1993.

Fudan University assisted in meeting the publication costs of this article.

REFERENCES

1. R. H. Wilson, R. W. Stoll, and M. A. Calcone, in *Proceedings of the Second International IEEE VLSI Multi-level Interconnect. Conference*, p. 343, Santa Clara, CA, June 25-26, 1985.
2. J. E. J. Schmitz, *Chemical Vapor Deposition of Tungsten and Tungsten Silicides for VLSI/ULSI Applications*, Chapter I, Noyes Publications, Park Ridge, NJ (1991).
3. E. K. Broadbent and C. L. Ramiller, *This Journal*, **131**, 1427 (1984).
4. W. T. Stocy, E. K. Broadbent, and M. H. Norcott, *ibid.*, **132**, 444 (1985).
5. M. L. Green and R. A. Levy, *ibid.*, **132**, 1243 (1985).
6. H. H. Busta and C. H. Tang, *ibid.*, **133**, 1195 (1986).
7. E. K. Broadbent, A. E. Morgan, J. M. DeBlasi, P. van der Putte, B. Coulman, B. J. Burrow, D. K. Sadana, and A. Reader, *ibid.*, **133**, 1715 (1986).
8. M. L. Green, Y. S. Ali, T. Boone, B. A. Davidson, L. C. Feldman, and S. Nakahara, *ibid.*, **134**, 2285 (1987).

9. M. Wong, N. Kobayashi, R. Browning, D. Paine, and K. C. Saraswat, *ibid.*, **134**, 2339 (1987).
10. N. Lifshitz, *Appl. Phys. Lett.*, **51**, 967 (1987).
11. H. J. Whitlow, Th. Eriksson, M. Ostling, C. S. Petersson, J. Keinonen, and A. Anttila, *ibid.*, **50**, 1497 (1987).
12. D. C. Paine, J. C. Bravman, and K. C. Saraswat, *Workshop on Tungsten and Other Refractory Metals for VLSI Applications*, R. S. Blewer, Editor, p. 117, MRS Conference Proceedings, Pittsburgh (1986).
13. J.-T. Wang, T. Andersson, and J.-O. Carlsson, *European Workshop on Refractory Metals and Silicides*, C. S. Petersson, Chairman, p. 1.7, Stockholm, March 24-27, 1991.
14. J.-T. Wang, in *Proceedings of the Third International Conference on Solid State and Integrated Circuit Technology*, R. Ellwanger *et al.*, Editors, p. 60, Beijing, Oct. 1992.
15. J.-T. Wang, K.-Y. Zhang, C.-B. Cao, and H. Wang, in *Proceedings of the Twelfth International Symposium on Chemical Vapor Deposition*, K. F. Jensen and G. W. Cullen, Editors, PV 93-2, p. 257, The Electrochemical Society Proceedings Series, Pennington, NJ (1993).
16. J.-T. Wang, K.-Y. Zhang, C.-B. Cao, H. Wang, and S.-L. Zhang, *ibid.*, p. 283.
17. J.-O. Carlsson and A. Harsta, *Thin Solid Films*, **158**, 107 (1988).
18. R. V. Joshi, V. Prasad, M. L. Yu, and G. Scilla, *J. Appl. Phys.*, **71**, 1428 (1992).
19. A. Kepten, A. Reisman, M. Ray, P. L. Smith, D. Temple, and F. Tapp, *This Journal*, **139**, 2331 (1992).

Low Voltage Cathodoluminescence of Mn²⁺-Activated ZnGa₂O₄

L. E. Shea,^a R. K. Datta,* and J. J. Brown, Jr.*

Center for Advanced Ceramic Materials, Virginia Polytechnic Institute and State University, Blacksburg, Virginia 24061

ABSTRACT

ZnGa₂O₄ and Zn_{1-x}Mn_xGa₂O₄ were investigated as potential low voltage cathodoluminescence phosphors for use in vacuum fluorescent displays. A low-voltage cathodoluminescence spectrophotometer was developed for phosphor characterization. Brightness was measured as a function of anode voltage (10 to 300 V). The effects of activator concentration, phosphor layer thickness, deposition process, and internal pressure were examined. The stability of these oxide phosphors in high vacuum and absence of corrosive gas emission under electron bombardment, offer advantages over commonly used sulfide phosphors.

Recently, there has been a renewed interest in the development of more efficient cathodoluminescent phosphors for use in computer screens, high definition television (HDTV), and vacuum fluorescent displays (VFDs).^{1,2} It is well known that for many years cathodoluminescent phosphors have been widely used in cathode ray tubes, image intensifiers, and television screens. However, the phosphors used in these applications require electron excitation voltages of 8,000 V or more to achieve adequate brightness. Such high voltages are impractical for the upcoming technology in the area of luminescence and display materials. For example, VFDs to be used as indicators on aircraft control panels or on automobile dashboards require 12 to 25 V dc for operation.² *The Washington Post* recently reported that by the next century, today's television sets will be outmoded and high definition cathode ray picture tubes will have arrived.¹ It has been reported that flat panel displays (FPDs) will soon begin replacing other displays on automobile dashboards, medical equipment, and aircraft.³

Sulfide-based phosphors such as ZnS:Cu,Al and (Zn,Cd)S:Ag,Cl are presently used in VFDs. These materials have been known to emit contaminant gases when bombarded by electrons.⁴⁻⁷ These gases proceed to corrode the oxide coating of the cathode filament, the most important VFD component and ultimately lead to filament deterioration. For this reason, an alternative to sulfide phosphors is needed. The present study focuses on ZnGa₂O₄ and Mn²⁺-activated ZnGa₂O₄. ZnGa₂O₄ is a self-activated phosphor that is blue-emitting under excitation by both ultraviolet light and low voltage electrons.⁴ Zn_{1-x}Mn_xGa₂O₄ emits green luminescence when excited by both ultraviolet light and low voltage electrons.^{8,9} Both of these phosphors crystallize in the spinel structure.

This study attempts to identify the experimental parameters required to achieve the maximum brightness under low voltage electron excitation for ZnGa₂O₄ and Zn_{1-x}Mn_xGa₂O₄. Brightness as a function of anode voltage, thickness of phosphor layer, phosphor deposition process, Mn²⁺ concentration, and internal pressure of the vacuum chamber was investigated.

* Electrochemical Society Active Member.

^a Present address: Materials Science Program, University of California San Diego, La Jolla, California 92093.

Experimental

Synthesis of phosphors.—Phosphors with the general formula Zn_{1-x}Mn_xGa₂O₄ were prepared by solid-state reaction techniques with *x* ranging from 0 to 0.03. The raw materials ZnO (Aldrich, 99.999%), Ga₂O₃ (Johnson-Matthey, 99.999%, metals basis), and MnO (Alfa, 99.5%) were thoroughly mixed under acetone in a glass mortar and pestle, allowed to dry, then fired in air at 1100°C for 17 h in covered alumina crucibles. After a light grinding and mixing step, the phosphor powders were placed in alumina boats, covered, and fired in a reducing atmosphere at 900°C for 1 h. After cooling, the phosphor powders were ground in an alumina mortar and pestle until the grain size was 7 to 10 μm. The particle size was measured using an Horiba LA-700 laser scattering particle size distribution analyzer.

X-ray diffraction measurements.—The phosphors were characterized by x-ray diffraction analysis using a Philips PW1729 x-ray diffractometer with Cu-K_α radiation operating at 40 kV, 30 mA, and 3°-2θ/min scanning rate.

Cathodoluminescence measurements.—The low voltage cathodoluminescence was measured at room temperature at 10⁻⁷ Torr with an in-house designed and assembled low voltage cathodoluminescence spectrophotometer. The capabilities of this instrument are summarized in Table I. A schematic diagram is shown in Fig. 1. Phosphor powder was deposited with thicknesses ranging from 2 to 6 mg/cm², on 4 × 4 mm indium tin oxide (ITO) conductive glass plates by a conventional sedimentation method in a solution of potassium silicate and barium acetate. After sedimentation, the wet phosphor screens were placed in a drying oven for 10 min at about 200°C. The cooled phosphor screens were immediately placed inside the vacuum chamber to be tested, to prevent absorption of water molecules from the ambient atmosphere. The conductive glass plate was posi-

Table I. Low voltage cathodoluminescent spectrophotometer capabilities.

Pressure	3.0 × 10 ⁻⁷ Torr
Anode voltage	10 to 300 V dc
Electron accelerating voltage	10 to 300 eV
Spot size	1 cm diam
Beam current	7 μA